Physics and Chemistry of Minerals manuscript No.
(will be inserted by the editor)

Anisotropic Diffusion of Water Molecules in Hydroxyapatite Nanopores

Muthuramalingam Prakash[a] · **Thibault Lemaire**[a] · **Matthieu Caruel,**[a] · **Marius Lewerenz**[c] · **Nora H. de Leeuw**[b] · **Devis Di Tommaso**[*,d] · **Salah Naili**[*,a]

Received: date / Accepted: date

Abstract New insights into the dynamical properties of water in hydroxyapatite (HAP) nanopores, a model systems for the fluid flow within nano-size spaces inside the collagen-apatite structure of bone, were obtained from molecular dynamics simulations of liquid water confined between two parallel HAP surfaces of different sizes (20 Å $\leq H \leq$ 240 Å). Calculations were conducted using a core-shell interatomic potential for HAP together with the extended simple point charge model for water. This force field gives an activation energy for water diffusion on the HAP surface that is in excellent agreement with available experimental data. The dynamical properties of water within the HAP nanopores were quantified in terms of the second-order water diffusion tensor. Results indicate that water diffuse anisotropically within the HAP nanopores with the solvent molecules moving parallel to the surface twice as fast as the perpendicular direction. This unusual dynamic behaviour is linked to the strong polarizing effect of calcium ions, and the synergic interactions between the water molecules in the first hydration layer of HAP with the calcium, hydroxyl and phosphate ions, which facilitate the flow of water molecules in the directions parallel to the HAP surface.

[a] Laboratoire Modélisation et Simulation Multi Echelle, MSME UMR 8208 CNRS, Université Paris-Est, 94010 Créteil Cedex, France. E-mail: salah.naili@univ-paris-est.fr
[b] School of Chemistry, Cardiff University, Main Building, Park Place, Cardiff CF10 3AT, United Kingdom.
[c] Laboratoire Modélisation et Simulation Multi Echelle, MSME UMR 8208 CNRS, Université Paris-Est, 77454 Marne la Vallée Cedex 2, France.
[d] School of Biological and Chemical Sciences, Queen Mary University of London, Mile End Road, E1 4NS London, United Kingdom. E-mail: d.ditommaso@qmul.ac.uk

Keywords Hydroxyapatite · Water Confinement · Molecular Dynamics · Hydrogen Bonding · Anisotropic Diffusion

Electronic supplementary material: The online version of this article (doi:10.1007/) contains supplementary material, which is available to authorized users.

1 Introduction

The macroscopic properties of bone tissue are tightly coupled to molecular processes taking place at the interface between Hydroxyapatite minerals (HAP, molecular unit formula $[Ca_{10}(PO_4)_6(OH)_2]$) and water within the lacuno-canalicular network (Sansalone et al 2013). In particular, the formulation of theoretical models for the prediction of tissue behaviour under the influence of time-dependent external stress inducing internal remodelling requires a detailed understanding of the dynamics of water and its interaction with the surface of HAP surfaces. Mechanics modelling for describing the mechanical behavior of bone at the macroscopic scale are based on homogenization and micromechanical methods which are powerful tools not only to obtain the overall behaviour of the material *via* the determination of the overall properties, but also to obtain information about the microfields which are defined at the microscale and are associated with the local distribution of the macrofields. Macroscopic predictions of either part or all of the elastic modulus tensor have been given by many authors (Yoon and Cowin 2008; Sansalone et al 2012; Hellmich and Katti 2015). In this context, bones with different forms of water will display differences in stiffness and strength.

HAP scaffolds constitute a prototypical model of biomaterial based surfaces (Kandori et al 2000b; Rimola et al 2012; Corno et al 2010) and have been used in several studies of bone repair (Oddou et al 2011). These substitutions HAP-based materials allowed the investigation of the interactions between HAP surfaces with biomolecules (Almora-Barrios et al 2009; Katti et al 2010; Kandori et al 2000a; Hernandez et al 2015; Lukasheva and Tolmachev 2015), water (Zhao et al 2014), ions (de Leeuw 2004a;b; Sakhno et al 2010) and gases (Chiatti et al 2013). Water plays a crucial role during bone mineralization and in the protein interaction (Corno et al 2010; Qin et al 2012; Nair et al 2014; Lemaire et al 2015a) as they can act as a prominent charge carrier, transporting ions (Prakash et al 2009; Prakash and Subramanian 2011) and maintaining the pH of the medium. When considering cells nanopores of transmembrane proteins (Hille 2001) or bone nanopores (Pham et al 2015), the interactions between water

molecules and the polar groups of HAP (calcium (Ca^{2+}), phosphate (PO_4^{3-}) and hydroxyl (OH^-) ions) may affect the local environment of the interface, modifying the diffusion of water molecules, which tend to be reduced when compared with the bulk (Bhide and Berkowitz 2005; von Hansen et al 2013; Lemaire et al 2015b).

The unusual dynamics of water and other molecules under confinement has been subject to several experimental and theoretical studies (Tan et al 2005; Sendner et al 2009; Su and Guo 2011; Nguyen and Bhatia 2012; Bourg and Steefel 2012; Srivastava et al 2012; Xu et al 2013; Planchais et al 2014; Prakash et al 2015; Han et al 2015; Qiu and Huang 2015; Nie et al 2016). In particular, nuclear magnetic resonance (NMR) techniques showed that water diffuses anisotropically inside nanoporous systems (Cleveland et al 1976; Thomsen et al 1987; Wei et al 2011; Salles et al 2011) and two different self-diffusion coefficients of water were measured in sheep Achilles tendon using pulsed-field-gradient stimulated-echo NMR (Fechete et al 2005). However, the molecular-level details regarding the diffusion mechanism of water molecules in the vicinity of the HAP bone surface, the origin of this anisotropic diffusion behaviour, and the interactions at the interface responsible for the preferential movement of water molecules towards a particular direction remain unclear.

Owing to advances in theoretical models and techniques, atomistic simulation methods are particularly suited to obtain a molecular-level characterization of the solid-water interface (Kirkpatrick et al 2005; Kubicki 2016), including a direct exploration of the structure and dynamics of water in contact with a mineral (Parvaneh et al 2016).

In this study, we present classical molecular dynamics (MD) simulations of liquid water in hydroxyapatite nanopores of different pore sizes. The aim of this work is to investigate the dynamical properties of water, and changes therein with varying pore size. In particular, the concept of self-diffusion tensor originally introduced by Kubo (1957) has been applied to compute all nine Cartesian components of the three dimensional diffusion. As the diffusion coefficient is a scalar quantity and cannot therefore determine the preferential movement of water molecules in a particular direction, in this work we computed the anisotropic diffusion of water within HAP nanopores to quantify the effect of confinement on its dynamic behaviour.

2 Theoretical models and methods

2.1 HAP surface and water models

Hydroxyapatite (HAP given by $Ca_{10}(PO_4)_6(OH)_2$) is viewed as an hexagonal primitive cell with $P6_3/m$ space group. The nanopore is represented by a face-to-face configuration of parallel HAP platelets. Its size corresponds to the narrowest pore diameters measured in bones by Holmes *et al.* (Holmes et al 1964). This geometrical configuration is motivated by the fact that, in bone tissue, hydroxyapatite is present in the form of thin micro-plates with dimensions ($L \times \ell \times e$), where $L = 250 - 500$ Å (in $\mathbf{e}_1$-direction), $\ell = 150 - 250$ Å (in $\mathbf{e}_2$-direction) and $e = 25$ Å (in $\mathbf{e}_3$-direction) (Weiner and Traub 1986). Cell parameters and crystallographic data of Sudarsanan and Young (Sudarsanan and Young 1969) are used for the initial configuration of the HAP structure. The dimensions of the parallelepipedic shaped simulation box were adjusted to contain $3 \times 3 \times 4$ such micro-plates. The position of each atom in the box is given using the vector position $\mathbf{r}$ whose the cartesian coordinates are denoted by (r_1, r_2, r_3) in the orthogonal frame $(\mathbf{e}_1, \mathbf{e}_2, \mathbf{e}_3)$ (see Fig. 1).

The HAP platelets and water layers constituted the elementary unit cell for our simulations. HAP nanopores were generated by varying the c-axis of the crystal from $H = 20$ Å to $H = 240$ Å. The resulting surface corresponds to the (0001) basal plane, which is the dominant surface in the thermodynamic morphology (Mkhonto and de Leeuw 2002) and important in biological systems, as the elongation of the bone platelets along the c-direction of the apatite crystal results in the expression of this surface (Rohanizadeh et al 1999). In addition, there is an experimental evidence that these faces act as the binding site for many adsorbates (Wierzbicki and Cheung 2000).

For all pore sizes, the atomic configuration editor Aten (Young 2016) was used to fill the resulting vacuum with water molecules corresponding to the experimental density of 1 g.cm^{-3}.

2.2 Molecular dynamics

All MD simulations were performed using the `DL_POLY` 4.05.1 program code (Todorov et al 2006). Interatomic potentials for HAP and its interaction with water are the ones developed by de Leeuw and Parker (de Leeuw 2004a; de Leeuw and Parker 1998). The water molecules were represented using the extended simple point charge

(SPC/E) potential (Berendsen et al 1981). The potential parameters used in this work are reported in electronic supporting material (see Tab. S1).

Each system considered in the present study was first equilibrated for 50 ps in the microcanonical (NVE) ensemble. This was followed by an equilibration period in the isothermal-isobaric (NPT) ensemble (P = 1 atm and T = 300 K) during which the volume was monitored in order to confirm the system reached equilibrium. The behaviour of the volume for the nanopores with H = 20 Å, 60 Å and 110 Å is reported in Fig. S2 of electronic supporting information. This was followed by 2 ns of production period in the NPT ensemble. All simulations used Nosé-Hoover algorithm with 0.5 ps and 0.5 ps as the thermostat and barostat relaxation times, respectively. To mimic the *in vivo* human bone environment, simulations were performed at temperature of 310 K unless otherwise stated. The Verlet leapfrog scheme with a time step of 0.1 fs was used to integrate the equations of motion. Periodic boundary conditions were applied in all three directions of the unit cell. The long range electrostatic interactions between the charges of all species were computed using the Smoothed Particle Mesh Ewald (SPME) method with a relative error of 10^{-6} (Essmann et al 1995). Table 1 lists the number of atoms in HAP (N_{HAP}), which included core-shell atoms, number of water molecules N_{O_w}, duration of each simulation T_D, and initial H and equilibrated H^* values of the pore sizes. Notice that the equilibrium height of the pore size is close to the initial one, which justifies the use of the the NPT ensemble instead of NVT for our simulations. The structure of the HAP nanopore-water systems considered in the present study are reported in Tab. S3 of electronic supporting material.

To verify if HAP nanopores and the surface retained the crystalline structure, we computed the phosphorous-phosphorous (P-P) radial distribution functions (RDFs) of the hydroxyapatite crystal, of the HAP nanopore (H = 110 Å) in contact with water, and of the surface of the HAP nanopore (see Fig. S4 of electronic supporting material). The P-P RDF profile of the nanopore is very similar to that of the crystal, which indicates that HAP nanopores remain crystalline. The P-P RDF profile of the HAP surface shows some deviations compared with that of HAP nanopore, suggesting some restructuring of the surface but not to an extend to indicate amorphousization of the surface. This also agrees with previous MD work by de Leeuw, which showed that HAP surfaces maintain its crystalline structure (de Leeuw 2004a) de Leeuw (2004b).

Table 1 Details of the molecular dynamics simulations of the HAP nanopores-water systems: number of atoms in HAP N_{HAP}, number of water molecules N_{O_w}, duration of each simulation T_D (in ns), initial H (in Å) and equilibrated H^* (in Å) pore sizes.

H (in Å)	N_{HAP}	N_{H_2O}	T_D (in ns)	H^* (in Å)
20	2520	455	2	21.6
30	2520	682	2	32.8
40	2520	910	2	41.3
50	2520	1138	2	52.7
60	2520	1363	2	64.1
70	2520	1593	2	71.4
80	2520	1820	2	82.7
90	2520	2048	2	92.4
100	2520	2276	2	103.9
110	2520	2506	2	112.6
120	2520	2732	2	124.6
130	2520	2960	2	135.3
160	2520	3650	1	167.3
200	2520	4550	1	196.8
240	2520	5300	1	228.1

2.3 Validation of the theoretical methodology

We have used the SPC/E water model because it gives a density, radial distribution functions, and self-diffusion coefficient for water in good agreement with experiment (Berendsen et al 1987). In particular, the value of self-diffusion coefficient D_s for bulk SPC/E water obtained from a molecular dynamics simulation of 729 water molecules (NPT ensemble, 2 ns of production period) is 2.58×10^9 m^2/s, in good agreement with the experimental value of 2.999×10^9 m^2/s (Holz et al 2000). Moreover, comprehensive calculations of the activation energy of diffusion E_a of water in bulk liquid water also concluded that using SPC/E model the value of E_a is 14.8 kJ/mol, which is only 2.6 kJ/mol lower than the experimental value E_a = 17.4 kJ/mol (Holmboe and Bourg 2014). To validate the combination of force fields, molecular models and computational techniques used in the present work, we compared the activation energy denoted E_a for the diffusion of water within HAP nanopores with the experimental values measured for cortical bone and inter-tubular dentine (Fernández-Seara et al 2002). MD simulations were conducted at the temperatures of 288, 298, 310 and 323 K to determine the activation energy for water diffusion in HAP nanopores with H = 60 Å and H = 110 Å (see Fig. 3), which are representative of typical nanopores in bones (50 < H < 125 Å) (Holmes et al 1964). The activation energies were obtained from the linear fit of the

points in Fig. 3 using Arrhenius equation $\ln(D_s) = \ln(D_0) - E_a/(RT)$, and the values of E_a are 22.5 ± 0.7 kJ/mol for $H = 60$ Å and 21.5 ± 2.0 kJ/mol for $H = 110$ Å, which are very close to experiments as seen for NMR measurements in cortical bone ($E_a = 26.6$ kJ/mol) and intertubular dentine $E_a = 29.5$ kJ/mol (Fernández-Seara et al 2002). This result validates the molecular models and interaction potentials used in the present work to represent fluid flow within bone sub-micrometer pores. A related point to consider is that the activation energies for water diffusion within the HAP nanopores are higher than in bulk $E_a = 17.4$ kJ/mol (Holmboe and Bourg 2014), which suggests that diffusion of water is hindered by the interaction between water molecules and the polar groups at the HAP surface.

3 Results and discussion

3.1 Self-diffusion coefficient

The self-diffusion coefficient of water, denoted by D_s, is a key property when studying the flow of fluid. From a MD simulation diffusion coefficients can be calculated using Einstein relation:

$$D_s = \frac{1}{d_s}\frac{1}{2}\frac{d\langle\langle[\mathbf{r}(t) - \mathbf{r}(0)]^2\rangle\rangle}{dt}. \tag{1}$$

where d_s is the dimension of the space (in this paper $d_s = 3$), $\mathbf{r}(0)$ and $\mathbf{r}(t)$ are the position vectors at times $t = 0$ and t, respectively, and the angled brackets $\langle\langle\cdot\rangle\rangle$ indicate the average over the number of times origin spanned by t and the number of water molecules. However, this scalar quantity can not describe the differential diffusion of water in directions parallel or perpendicular to the HAP surface in Fig. 1.

In order to quantify the anisotropic diffusion of water in the HAP nanopores, we introduce the second order water self-diffusion tensor $\mathbf{D}$, which is defined as:

$$\mathbf{D} = \begin{pmatrix} D_{11} & D_{12} & D_{13} \\ D_{12} & D_{22} & D_{23} \\ D_{13} & D_{23} & D_{33} \end{pmatrix}, \tag{2}$$

whose components D_{ij} represent the anisotropic diffusion coefficients and are computed using the following expression which is derived from (Kubo 1957):

$$D_{ij} = \frac{1}{2}\frac{d\langle\langle |r_i(t) - r_i(0)| \cdot |r_j(t) - r_j(0)| \rangle\rangle}{dt}, \qquad i, j = 1, 2, 3. \tag{3}$$

In Eq. (3), $r_i(0)$ and $r_i(t)$ are the components of the position vectors along the $\mathbf{e}_i$-direction ($i, j = 1, 2, 3$) of the Cartesian frame shown in Fig. 1. The anisotropic diffusion coefficients D_{ij} were computed by modifying the DL-POLY code. This new utility accurately determines the anisotropic self-diffusion coefficients by computing the mean square displacement (MSD) for the different atomic species in the simulation using multiple time origins as defined by Eq. 3. The mean square displacements associated with the diagonal elements of the anisotropic self-diffusion tensor D_{ii} for $i = 1, 2, 3$ are plotted in the Fig. 2.

Without attempting an exhaustive list on a subject beyond the scope of this paper, Cummings *et al.* (Cummings et al 1991) have presented different methods for calculating certain self-diffusion coefficients in a non-newtonian fluid subject to a couette strain field. Furthermore, Liu *et al.* (Liu et al 2004) have introduced a Einstein-Smoluchowski like method for calculating the parallel and perpendicular components of the self-diffusion to a surface. Boţan *et al.* (Boţan et al 2011) have used this previous method for studying the self-diffusion in clay nanopores.

The anisotropic diffusion tensor $\mathbf{D}$ can be decomposed into its so-called spherical and deviatoric parts:

$$\mathbf{D} = \frac{1}{3}(\mathrm{Tra}\ \mathbf{D})\,\mathbf{I} + \mathrm{Dev}\ \mathbf{D}, \tag{4}$$

where $\mathbf{I}$ is the identity tensor, Tra is trace operator that gives the sum of the diagonal elements of $\mathbf{D}$, and the deviatoric part is given by $\mathrm{Dev}\ \mathbf{D} = \mathbf{D} - (1/3)(\mathrm{Tra}\ \mathbf{D})\,\mathbf{I}$. Any tensor of the form $\alpha\mathbf{I}$, where α is a scalar, is known as a spherical tensor, while Dev $\mathbf{D}$ is known as a deviator of $\mathbf{D}$. Note that an important property of the deviatoric tensors is Tra (Dev $\mathbf{D}$) = 0. This decomposition decouples the "volumetric" from the "distortional" properties which can be interpreted as a decoupling of the "mean" part from the "fluctuation" part because of the underlying orthogonality of the spherical and deviatoric partitions $\mathrm{Tra}\ (\mathbf{D}_s \times \mathrm{Dev}\ \mathbf{D}) = 0$, where $\mathbf{D}_s = (1/3)(\mathrm{Tra}\ \mathbf{D})\,\mathbf{I}$. This decomposition mimics the ones of the vectors that can be decomposed uniquely as a sum of two vectors, one tangent to a surface, called the tangential component of the vector, and another one perpendicular to the surface,

called the normal component of the vector. As a result due to the geometry of the HAP nanopores, the matrix representation of the self-diffusion tensor **D** should be diagonal. This was first confirmed by the obtention of the quasi-nullity of the off-diagonal elements, and then by computing the spherical part of **D** in Eq. (4), which does indeed correspond to the standard diffusion coefficient of water calculated using Eq. (1).

The anisotropic diffusion coefficients of water as a function of the pore size are reported in Fig. 4. Our calculations show that the transport properties of water depend significantly on the size of the HAP nanopore (Pham et al 2015), but also quantify the marked anisotropic behaviour of liquid water when confined within nano-size volumes.

In Fig. 4, for small to medium nanopores (20 Å $< H <$ 70 Å) the coefficients D_{11} and D_{22} associated with the diffusion along the $\mathbf{e}_1$ and $\mathbf{e}_2$ directions, correspond to the movement of particles parallel to the HAP surface (see Fig. 1), and their values are similar to to the isotropic self-diffusion coefficient D_s. For nanopores larger than $>$ 70 Å, D_{11} is about 15% higher than D_s, whereas $D_{22} \sim D_s$. On the other hand, for all nanopores the coefficients D_{33}, which correspond to the normal direction to the HAP surface, are significantly lower than both the isotropic coefficient D_s, and the coefficients D_{11} and D_{22} associated with the diffusion parallel to the HAP surface. For example, in the HAP nanopore with H = 110 Å, $D_{33} = 1.5 \times 10^{-9}$ m^2/s and D_{11} and D_{22} are equal to 3.0×10^{-9} m^2/s and 2.2×10^{-9} m^2/s, respectively. This signifies that water molecules preferentially diffuse along the HAP surfaces rather than towards the bulk of the aqueous solution in contact with the nanopore. In Fig. 4 also notice spherical part of the diffusion tensor **D** corresponds to the standard isotropic diffusion coefficient.

This in-plane confinement effect is visually represented in Fig. 5 by the trajectory of a water molecules that is part of the first hydration layer of the HAP nanopore with H = 110 Å. A water molecule was considered to be part of the first hydration layer of HAP if the distance between the calcium atoms (Ca) at the HAP surface and the oxygen atoms (O_w) of the water molecules is less than 3.0 Å. This distance corresponds to the position of the first minimum in the $Ca^{2+} - O_w$ pair distribution function (*e.g.*, Di Tommaso *et al.* (Di Tommaso et al 2014)) as well as the position of the minimum in the number density profile of the oxygen atoms that is closer to the HAP surface (see Fig. 5). This graph shows that during the dynamics the tagged water molecule moves approximately parallel to the surface of HAP. A similar conclusion were obtained from the visualization of the trajectories of water molecules that were part of the second hydration layer of HAP. Moreover, the analysis of the motion of the tracer molecule from its initial (t = 0 ns) to its final (t = 2 ns) MD steps indicates that the $\mathbf{e}_1$ and $\mathbf{e}_2$ components of

the position vector change by twice as much as the $\mathbf{e}_3$ component. This agrees with the values of the anisotropic diffusion coefficients D_{11} and D_{22} being larger than D_{33} (see Fig. 4). The polarization effect of the calcium ions at the HAP surface, which can extend up to four layers of water (Bolis et al 2012), can help rationalize the slow diffusion of water along the $\mathbf{e}_3$-direction observed in our MD simulations.

The time-dependent mean square displacement (MSD) of the oxygen atoms of water molecules (O_w) close to the HAP-water interface and further away from it was also computed using the following expression:

$$\langle\langle \Delta\mathbf{r}^2(t)\rangle\rangle_{O_{w,n}} = \langle\langle[\mathbf{r}(t) - \mathbf{r}(0)]^2\rangle\rangle,$$

where $\mathbf{r}(0)$ and $\mathbf{r}(t)$ are the position vectors at times $t = 0$ and t, respectively, and the angled brackets $\langle\langle\cdot\rangle\rangle$ indicate the average over the number of times origin spanned by t and the number of water molecules. The subscript $O_{w,n}$ denotes the oxygen atoms that are part of the n-th "layer" of water in the HAP nanopore. For example, a water molecule was considered to be part of the first hydration layer if $d(Ca^{2+} - O_w) < 3.0$ Å. The (water) oxygen atoms used to compute the MSD of a specific hydration layer were determined from the configuration of the first MD step of the production period and by selecting those O_w atoms such that the $d(Ca^{2+} - O_w)$ was within a specific threshold. The MSD of O_w in the hydroxyapatite nanopores with $H = 60$ Å and 110 Å for hydration layers defined by $d(Ca^{2+} - O_w)$ thresholds equal to 6 Å (first and second layer), 20 Å, 30 Å and 40 Å are reported in Fig. S5 of electronic supporting material. Results indicate that as we move further away from the interface, water molecules diffuse more slowly and this effect becomes more pronounced with the size of the nanopore. However, it is important to notice that several water exchanges could be counted between the different hydration layers during the MD trajectories, and consequently the MSD in Fig. S4 cannot be unambiguously associated to a specific hydration layer of the HAP nanopore.

3.2 Hydrogen bonding at the HAP-water interface

Hydrogen bonding (H-bonding) interactions play a vital role in the movement of water molecules on the HAP surface. Figure 6 shows the molecular arrangement of water molecules on the HAP surface. In particular, Fig. 6(a) gives a closer view of the orientation of water molecules on the surface and the H-bonded interaction with hydroxyl and phosphate groups of HAP. Visualization of the trajectories revealed a peculiar "rolling" motion for the water

molecules. This is illustrated in Fig. 6(b)-(e), where the molecular arrangement of a selected water molecule at four MD steps shows that the H-bonding interactions with the HAP surface influence the translation and rotation motions of water and facilitate the anisotropic diffusion of water. Figure 7 reports a schematic representation of the rolling motion of water, which occurs *via* H-bonding interactions determining the preferential diffusion of water molecules on the $(\mathbf{e}_1, \mathbf{e}_2)$-plane.

The H-bonding structure greatly influences the dynamical properties of water (Chandra 2002). The effect of confinement on the distribution of the number of H-bonds was therefore quantified by scanning the MD trajectories of bulk liquid water and HAP nanopores to determine the existence of an H-bond between two water molecules based on the following geometrical criteria: (i) the donor-acceptor inter-oxygen distance is less than 3.5 Å; (ii) the donor acceptor inter hydrogen-oxygen distance is less than 2.45 Å; (iii) the hydrogen-donor-acceptor angle is less than 30° (Chandra 2000).

The average number of H-bonds n_{HB} is about 3.5 in bulk liquid water and in the HAP nanopore with $H = 110$ Å but n_{HB} decreases to 3.4 for $H = 60$ Å, 3.3 for $H = 40$ Å and 3.0 for $H = 20$ Å, that is, as the degree of confinement increases. This is linked with the influence of the HAP surface on H-bonding network. In fact, the distribution of the number of H-bonds between water molecules coordinated to the HAP surface and the surrounding water molecules (see Tab. 2) shows that in liquid water the majority of water molecules (51%) are in the ideal local tetrahedral network, whereas in the first hydration layer of HAP more than 60% of water molecules have two, one or zero H-bonds. Since in an aqueous environment the motion of water molecules occurs *via* the breaking and reforming of H-bonds, the reduction in water diffusion within HAP nanopores can be explained in terms of the lack of water-water H-bonds through which a water molecule can diffuse from the surface to the bulk. Since the molecules coordinated on the surface form, on average, less than two HBs per molecule with the surrounding water molecules, this implies that they interact with the hydroxyl group and diffuse preferentially along the surface rather than towards the bulk solution.

4 Conclusion

We conducted classical molecular dynamics simulations of liquid water within hydroxyapatite nanopores of different sizes (20 Å $\leq H \leq$ 240 Å) in order to determine the effect of confinement on the dynamical properties of

Table 2 Distribution of the number of hydrogen-bonds for the water molecules coordinated to the calcium surfaces. Results obtained from molecular dynamics simulations of bulk water and water within HAP nanopores of different sizes (20 Å$\leq H \leq$ 110 Å). The values given are percentages of molecules with the given number of hydrogen bonds and the average number of hydrogen bonds per water molecule.

	0	1	2	3	4	5	Average
Bulk water	0.0	0.9	0.8	33.0	51.3	5.9	3.53
HAP-water							
110 Å	22.3	22.4	22.0	19.7	12.5	1.0	1.81
60 Å	22.7	22.5	22.0	19.4	12.3	1.0	1.79
40 Å	24.5	23.6	21.4	18.3	11.2	1.0	1.71
20 Å	26.8	27.9	21.2	15.0	8.3	0.7	1.52

water. We showed that our core-shell potential for hydroxyapatite together with the standard SPC/E water model gives an activation energy for water diffusion of water on the hydroxyapatite surface that is in good agreement with available experimental data. We identified an anisotropic diffusive behaviour for the molecules, which was quantified by defining a self-diffusion tensor, **D**, and computing the anisotropic diffusion coefficients of water, D_{ij} ($i, j = 1,2,3$). As a result of the strong interactions between water molecules and the functional groups of HAP, which become dominant in such confined environments, the motion of water molecules in the direction parallel to the surface is significantly faster than in the direction perpendicular to it, where the polarizing effect of Ca^{2+} sites reduces the diffusion of water molecules. On the other hand, solvent molecules can move preferentially along the $\mathbf{e}_1$-direction (characterized by anisotropic diffusion coefficient D_{11}) as a result of synergic interactions of the water molecules at the interface with the calcium, hydroxyl and phosphate ions of the HAP surface.

Our study demonstrates and quantifies the anisotropic behaviour of fluid in bone nanostructures, which is an important area of bone biophysics (Lemaire et al 2015a; Abdalrahman et al 2015), and therefore gives new insights into the mechanisms controlling the motion of solvent molecules in confined spaces.

Acknowledgements The authors are grateful to the "Institut des sciences de l'ingénierie et des systèmes" (INSIS) of the "Centre national de la recherche scientifique" (CNRS) for financial support through the "HAP-W Nanopores" PEPS grant. The authors are also grateful to "Université Paris-Est Créteil" (UPEC) for the support of the French-English consortium. Finally, Dr Muthuramalingam Prakash thanks UPEC for the funding of his post-doctoral research grant. This research utilised Queen Mary's MidPlus computational facilities, supported by QMUL Research-IT and funded by EPSRC grant EP/K000128/1.

Conflict of interest

The authors declare that they have no conflict of interest.

References

Abdalrahman T, Scheiner S, Hellmich C (2015) Is trabecular bone permeability governed by molecular ordering-induced fluid viscosity gain? arguments from re-evaluation of experimental data in the framework of homogenization theory. J Theor Biol 365:433–444

Almora-Barrios N, Austen KF, de Leeuw NH (2009) Density functional theory study of the binding of glycine, proline, and hydroxyproline to the hydroxyapatite (0001) and (0110) surfaces. Langmuir 25(9):5018–5025

Berendsen H, Grigera J, Straatsma T (1987) The missing term in effective pair potentials. J Phys Chem 91(24):6269–6271

Berendsen HJ, Postma JP, van Gunsteren WF, Hermans J (1981) Interaction models for water in relation to protein hydration. In: Intermolecular forces, Springer, pp 331–342

Bhide SY, Berkowitz ML (2005) Structure and dynamics of water at the interface with phospholipid bilayers. J Chem Phys 123(22):224,702

Boţan A, Rotenberg B, Marry V, Turq P, Noetinger B (2011) Hydrodynamics in clay nanopores. J Phys Chem C 115:16,109–16,115

Bolis V, Busco C, Martra G, Bertinetti L, Sakhno Y, Ugliengo P, Chiatti F, Corno M, Roveri N (2012) Coordination chemistry of ca sites at the surface of nanosized hydroxyapatite: interaction with H_2O and CO. Philos T Roy Soc A 370(1963):1313–1336

Bourg IC, Steefel CI (2012) Molecular dynamics simulations of water structure and diffusion in silica nanopores. J Phys Chem C 116(21):11,556–11,564

Chandra A (2000) Effects of ion atmosphere on hydrogen-bond dynamics in aqueous electrolyte solutions. Phys Rev Lett 85:768–771

Chandra A (2002) Structure and dynamics of hydrogen bonds in liquid water and aqueous solutions. Proc Indian Natn Sci Acad 69:49–69

Chiatti F, Corno M, Sakhno Y, Martra G, Ugliengo P (2013) Revealing hydroxyapatite nanoparticle surface structure by CO adsorption: A combined B3LYP and infrared study. J Phys Chem C 117(48):25,526–25,534

Cleveland G, Chang D, Hazlewood C, Rorschach H (1976) Nuclear magnetic resonance measurement of skeletal muscle: anisotrophy of the diffusion coefficient of the intracellular water. Biophys J 16(9):1043–1053

Corno M, Rimola A, Bolis V, Ugliengo P (2010) Hydroxyapatite as a key biomaterial: quantum-mechanical simulation of its surfaces in interaction with biomolecules. Phys Chem Chem Phys 12(24):6309–6329

Cummings P, Wang B, Evans D, Fraser K (1991) Nonequilibrium molecular dynamics calculation of self-diffusion in a non-newtonian fluid subject to a couette strain field. J Chem Phys 94(3):2149–2158

Di Tommaso D, Ruiz-Agudo E, de Leeuw NH, Putnis A, Putnis CV (2014) Modelling the effects of salt solutions on the hydration of calcium ions. Phys Chem Chem Phys 16:7772–7785

Essmann U, Perera L, Berkowitz ML, Darden T, Lee H, Pedersen LG (1995) A smooth particle mesh ewald method. J Chem Phys 103(19):8577–8593

Fechete R, Demco D, Eliav U, Blümich B, Navon G (2005) Self-diffusion anisotropy of water in sheep achilles tendon. NMR Biomed 18(8):577–586

Fernández-Seara MA, Wehrli SL, Wehrli FW (2002) Diffusion of exchangeable water in cortical bone studied by nuclear magnetic resonance. Biophys J 82(1):522–529

Han KN, Bernardi S, Wang L, Searles DJ (2015) Water diffusion in zeolite membranes: Molecular dynamics studies on effects of water loading and thermostat. J Membr Sci 495:322–333

von Hansen Y, Gekle S, Netz RR (2013) Anomalous anisotropic diffusion dynamics of hydration water at lipid membranes. Phys Rev Lett 111(11):118,103

Hellmich C, Katti D (2015) Multiscale mechanics of biological, bioinspired, and biomedical materials. MRS Bull 40(04):309–313

Hernandez SER, Streeter I, de Leeuw NH (2015) The effect of water on the binding of glycosaminoglycan saccharides to hydroxyapatite surfaces: a molecular dynamics study. Phys Chem Chem Phys 17(34):22,377–22,388

Hille B (2001) Ion channels of excitable membranes, vol 507. Sinauer Sunderland, MA

Holmboe M, Bourg IC (2014) Molecular dynamics simulations of water and sodium diffusion in smectite interlayer nanopores as a function of pore size and temperature. J Phys Chem C 118:1001–1013

Holmes J, Davies D, Meath W, Beebe R (1964) Gas adsorption and surface structure of bone mineral. Biochem 3(12):2019–2024

Holz M, Heil SR, Sacco A (2000) Temperature-dependent self-diffusion coefficients of water and six selected molecular liquids for calibration in accurate 1H NMR PFG measurements. Phys Chem Chem Phys 2:4740–4742

Kandori K, Fudo A, Ishikawa T (2000a) Adsorption of myoglobin onto various synthetic hydroxyapatite particles. Phys Chem Chem Phys 2(9):2015–2020

Kandori K, Mukai M, Yasukawa A, Ishikawa T (2000b) Competitive and cooperative adsorptions of bovine serum albumin and lysozyme to synthetic calcium hydroxyapatites. Langmuir 16(5):2301–2305

Katti KS, Pradhan SM, Katti DR (2010) Mechanics of collagen in the human bone: role of collagen-hydroxyapatite interactions. In: MRS Proceedings, Cambridge Univ Press, vol 1274, pp 1274–QQ06–03

Kirkpatrick R, Kalinichev A, Wang J (2005) Molecular dynamics modelling of hydrated mineral interlayers and surfaces: structure and dynamics. Mineral Mag 69(3):289–308, URL http://www.ingentaconnect.com/content/minsoc/mag/2005/00000069/00000003/art00005

Kubicki J (ed) (2016) Molecular modeling of geochemical reactions: an introduction. Wiley

Kubo R (1957) Statistical-mechanical theory of irreversible processes. I. General theory and simple applications to magnetic and conduction problems. Journal of the Physical Society of Japan 12(6):570–586

de Leeuw NH (2004a) A computer modelling study of the uptake and segregation of fluoride ions at the hydrated hydroxyapatite (0001) surface: introducing a $Ca_{10}(PO_4)_6(OH)_2$ potential model. Phys Chem Chem Phys 6(8):1860–1866

de Leeuw NH (2004b) Resisting the onset of hydroxyapatite dissolution through the incorporation of fluoride. J Phys Chem B 108(6):1809–1811

de Leeuw NH, Parker S (1998) Molecular-dynamics simulation of MgO surfaces in liquid water using a shell-model potential for water. Phys Rev B 58(20):13,901

Lemaire T, Pham T, Capiez-Lernout E, de Leeuw N, Naili S (2015a) Water in hydroxyapatite nanopores: possible implications for interstitial bone fluid flow. J Biomech 48(12):3066–3071

Lemaire T, Pham TT, de Leeuw N, Naili S (2015b) Bone water at the nanoscale: a molecular dynamics study. Comput Methods Biomech Biomed Engin 18(sup1):1982–1983

Liu P, Harder E, Berne B (2004) On the calculation of diffusion coefficients in confined fluids and interfaces with an application to the liquid-vapor interface of water. J Phys Chem B 108:6595–6602

Lukasheva NV, Tolmachev DA (2015) Cellulose nanofibrils and mechanism of their mineralization in biomimetic synthesis of hydroxyapatite/native bacterial cellulose nanocomposites: Molecular dynamics simulations. Langmuir 32(1):125–134

Mkhonto D, de Leeuw NH (2002) A computer modelling study of the effect of water on the surface structure and morphology of fluorapatite: introducing a $Ca_{10}(PO_4)6F_2$ potential model. J Mater Chem 12:2633–2642

Nair AK, Gautieri A, Buehler MJ (2014) Role of intrafibrillar collagen mineralization in defining the compressive properties of nascent bone. Biomacromolecules 15(7):2494–2500

Nguyen TX, Bhatia SK (2012) Some anomalies in the self-diffusion of water in disordered carbons. J Phys Chem C 116(5):3667–3676

Nie GX, Wang Y, Huang JP (2016) Shape effect of nanochannels on water mobility. Frontiers of Physics 11(6):1–8

Oddou C, Lemaire T, Pierre J, David B (2011) Hydrodynamics in porous media with applications to tissue engineering. In: Vafai K (ed) Porous media: applications in biological systems and biotechnology, CRC Press, pp 75–119

Parvaneh L, Donadio D, Sulpizi M (2016) Molecular mechanism of crystal growth inhibition at the calcium oxalate/water interfaces. The Journal of Physical Chemistry C 120(8):4410–4417

Pham TT, Lemaire T, Capiez-Lernout E, Lewerenz M, To QD, Christie JK, Di Tommaso D, de Leeuw NH, Naili S (2015) Properties of water confined in hydroxyapatite nanopores as derived from molecular dynamics simulations. Theo Chem Acc 134(5):1–14

Planchais A, Devautour-Vinot S, Salles F, Ragon F, Devic T, Serre C, Maurin G (2014) A joint experimental/computational exploration of the dynamics of confined water/zr-based mofs systems. J Phys Chem C 118(26):14,441–14,448

Prakash M, Subramanian V (2011) Structure, stability and spectral signatures of monoprotic carborane acid–water clusters (CBWn, where n= 1–6). Phys Chem Chem Phys 13(48):21,479–21,486

Prakash M, Subramanian V, Gadre SR (2009) Stepwise hydration of protonated carbonic acid: a theoretical study. J Phys Chem A 113(44):12,260–12,275

Prakash M, Jobic H, Ramsahye NA, Nouar F, Damasceno Borges D, Serre C, Maurin G (2015) Diffusion of H_2, CO_2, and their mixtures in the porous Zirconium based metal–organic framework MIL-140A(Zr): Combination of quasi-elastic neutron scattering measurements and molecular dynamics simulations. J Phys Chem C 119(42):23,978–23,989

Qin Z, Gautieri A, Nair AK, Inbar H, Buehler MJ (2012) Thickness of hydroxyapatite nanocrystal controls mechanical properties of the collagen–hydroxyapatite interface. Langmuir 28(4):1982–1992

Qiu T, Huang JP (2015) Unprecedentedly rapid transport of single-file rolling water molecules. Frontiers of Physics 10:1–8

Rimola A, Corno M, Garza J, Ugliengo P (2012) *Ab initio* modelling of protein–biomaterial interactions: influence of amino acid polar side chains on adsorption at hydroxyapatite surfaces. Philos T Roy Soc A 370(1963):1478–1498

Rohanizadeh R, Trécant-Viana M, Daculsi G (1999) Ultrastructural study of apatite precipitation in implanted calcium phosphate ceramic: Influence of the implantation site. Calcif Tissue Int 64(5):430–436

Sakhno Y, Bertinetti L, Iafisco M, Tampieri A, Roveri N, Martra G (2010) Surface hydration and cationic sites of nanohydroxyapatites with amorphous or crystalline surfaces: a comparative study. J Phys Chem C 114(39):16,640–16,648

Salles F, Bourrelly S, Jobic H, Devic T, Guillerm V, Llewellyn P, Serre C, Ferey G, Maurin G (2011) Molecular insight into the adsorption and diffusion of water in the versatile hydrophilic/hydrophobic flexible MIL-53(Cr) MOF. J Phys Chem C 115(21):10,764–10,776

Sansalone V, Naili S, Lemaire T (2012) Nanostructure and effective elastic properties of bone fibril. Bioinspir Biomim Nanobiomaterials 1(3):154–165

Sansalone V, Kaiser J, Naili S, Lemaire T (2013) Interstitial fluid flow within bone canaliculi and electro-chemo-mechanical features of the canalicular milieu. Biomechanics and modeling in mechanobiology 12(3):533–553

Sendner C, Horinek D, Bocquet L, Netz RR (2009) Interfacial water at hydrophobic and hydrophilic surfaces: Slip, viscosity, and diffusion. Langmuir 25(18):10,768–10,781

Srivastava R, Singh JK, Cummings PT (2012) Effect of electric field on water confined in graphite and mica pores. J Phys Chem C 116(33):17,594–17,603

Su J, Guo H (2011) Effect of nanotube-length on the transport properties of single-file water molecules: transition from bidirectional to unidirectional. J Chem Phys 134(24):244,513

Sudarsanan KT, Young R (1969) Significant precision in crystal structural details. holly springs hydroxyapatite. Acta Crystallogr Sect B 25(8):1534–1543

Tan HS, Piletic IR, Fayer M (2005) Orientational dynamics of water confined on a nanometer length scale in reverse micelles. J Chem Phys 122(17):174,501

Thomsen C, Henriksen O, Ring P (1987) *In vivo* measurement of water self diffusion in the human brain by magnetic resonance imaging. Acta Radiol 28(3):353–361

Todorov IT, Smith W, Trachenko K, Dove MT (2006) DL-POLY 3: new dimensions in molecular dynamics simulations via massive parallelism. J Mater Chem 16(20):1911–1918

Wei MJ, Zhou J, Lu X, Zhu Y, Liu W, Lu L, Zhang L (2011) Diffusion of water molecules confined in slits of rutile TiO_2 (110) and graphite (0001). Fluid Phase Equilib 302(1):316–320

Weiner S, Traub W (1986) Organization of hydroxyapatite crystals within collagen fibrils. FEBS LETT 206:262–266

Wierzbicki A, Cheung HS (2000) Molecular modeling of inhibition of hydroxyapatite by phosphocitrate. J Mol Struct (THEOCHEM) 73(1-3):73–82

Xu L, Hu YZ, Ma TB, Wang H (2013) Tunable giant anisotropic diffusion of water sub-monolayers between graphene layers. Nanotechnol 24(50):505,504

Yoon YJ, Cowin SC (2008) The estimated elastic constants for a single bone osteonal lamella. Biomech Model Mechanobiol 7(1):1–11

Young T (2016) Aten. coordinate creator and editor for atomistic simulations, including periodic systems. URL https://www.projectaten.com

Zhao W, Xu Z, Yang Y, Sahai N (2014) Surface energetics of the hydroxyapatite nanocrystal–water interface: A molecular dynamics study. Langmuir 30(44):13,283–13,292

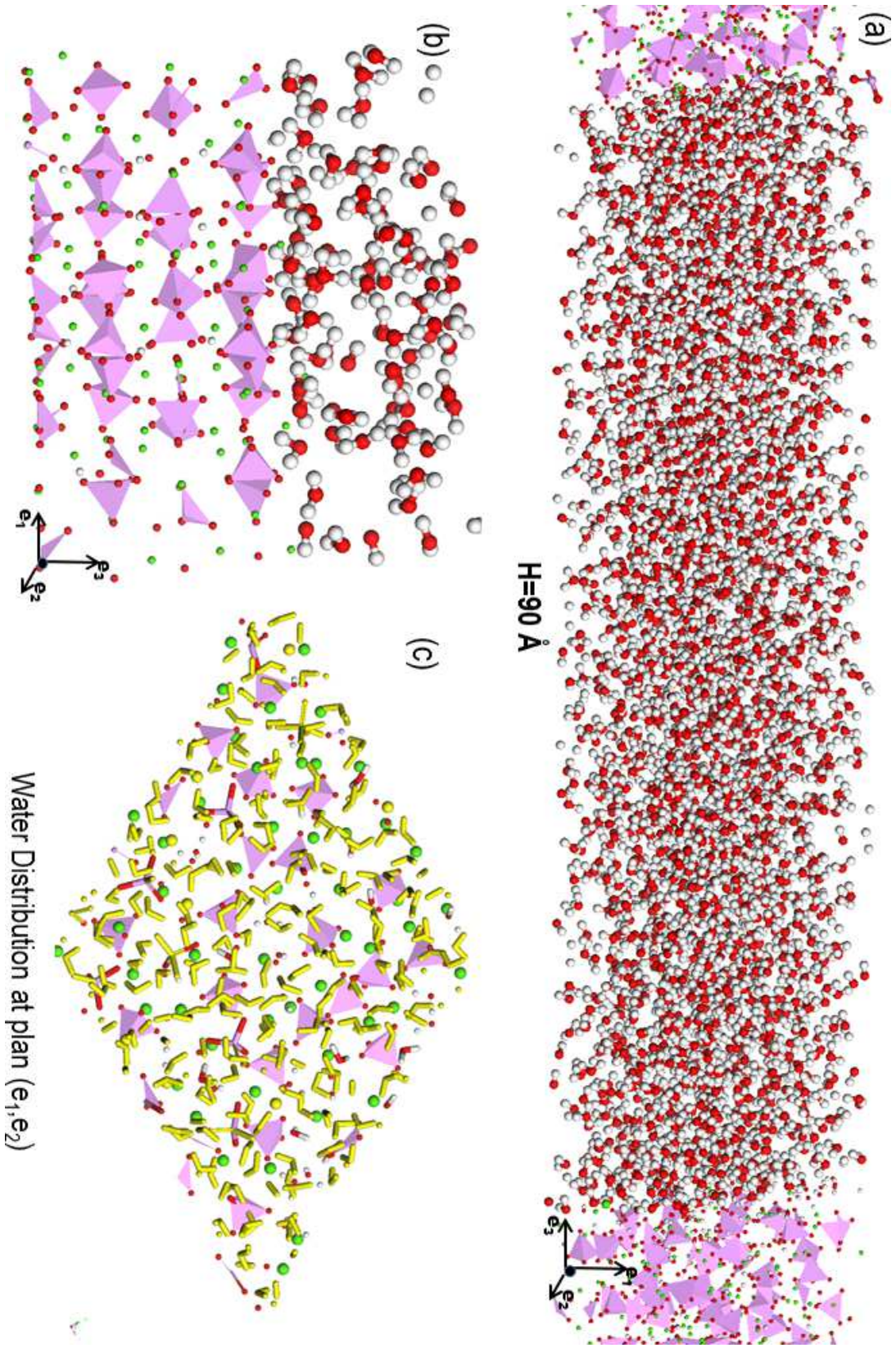

Fig. 1 HAP-water system (Ca-green, PO_4^{3-}-pink, O-red, H-white) with a pore size of 90 Å.

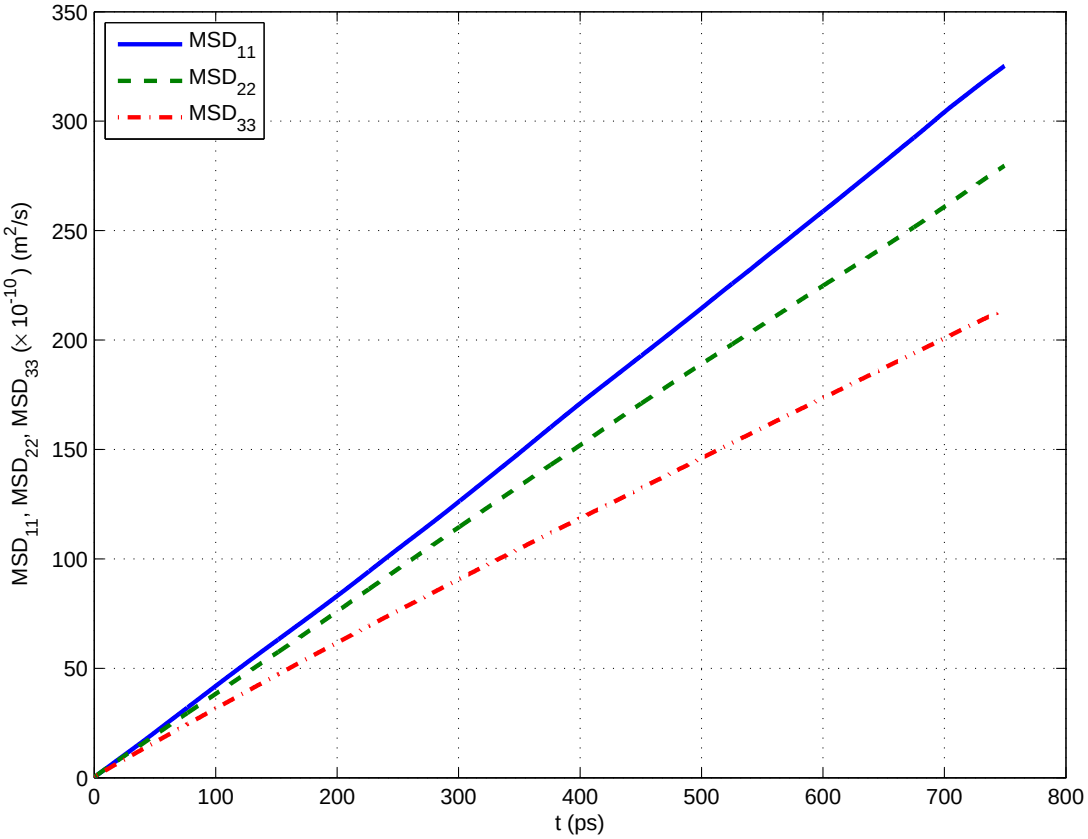

Fig. 2 The mean square displacements associated with the three interest quantities describing the diffusion coefficients D_{ii} for $i = 1,2,3$ for $H = 90$ Å.

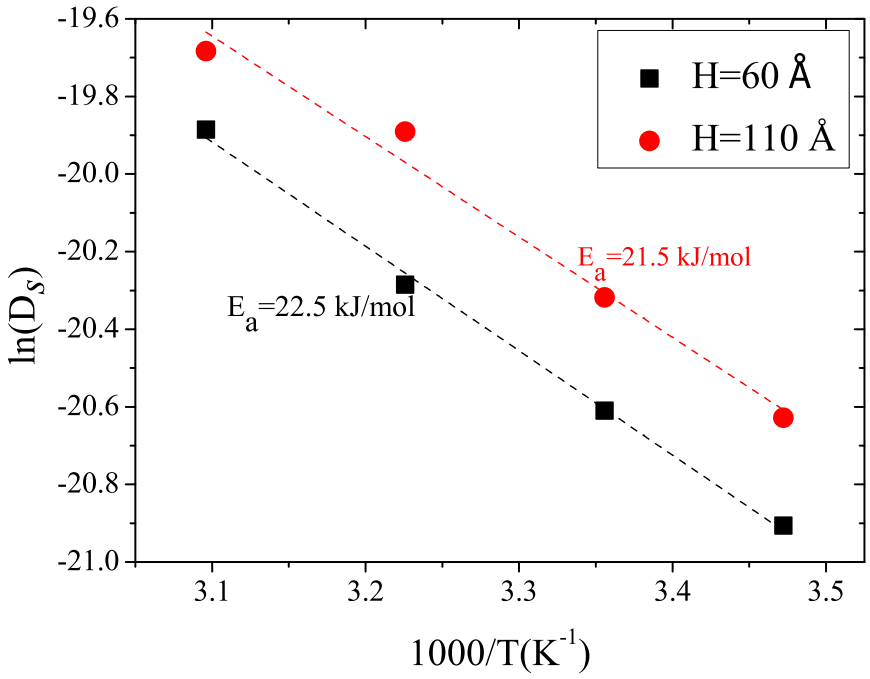

Fig. 3 Arrhenius plots of the average diffusion coefficient of water *versus* the inverse of the temperature for the HAP-water systems with pore sizes equal to 60 Å and 110 Å where H is the initial height of the nanopore.

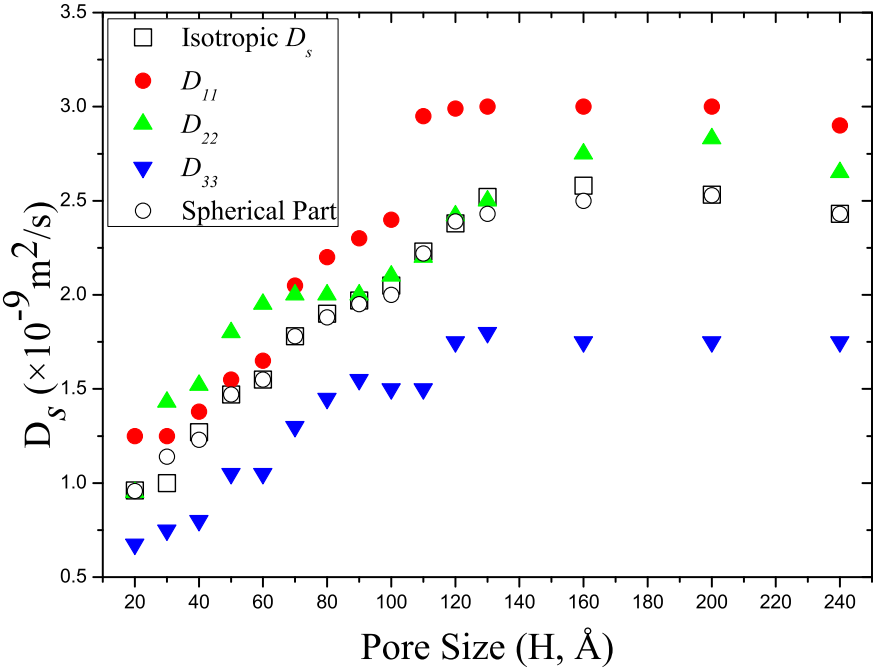

Fig. 4 Anisotropic diffusion coefficients D_{ii} (i = 1, 2, 3), standard isotropic diffusion coefficient D_s, and spherical part of the diffusion tensor **D** of water molecules within the HAP nanopores.

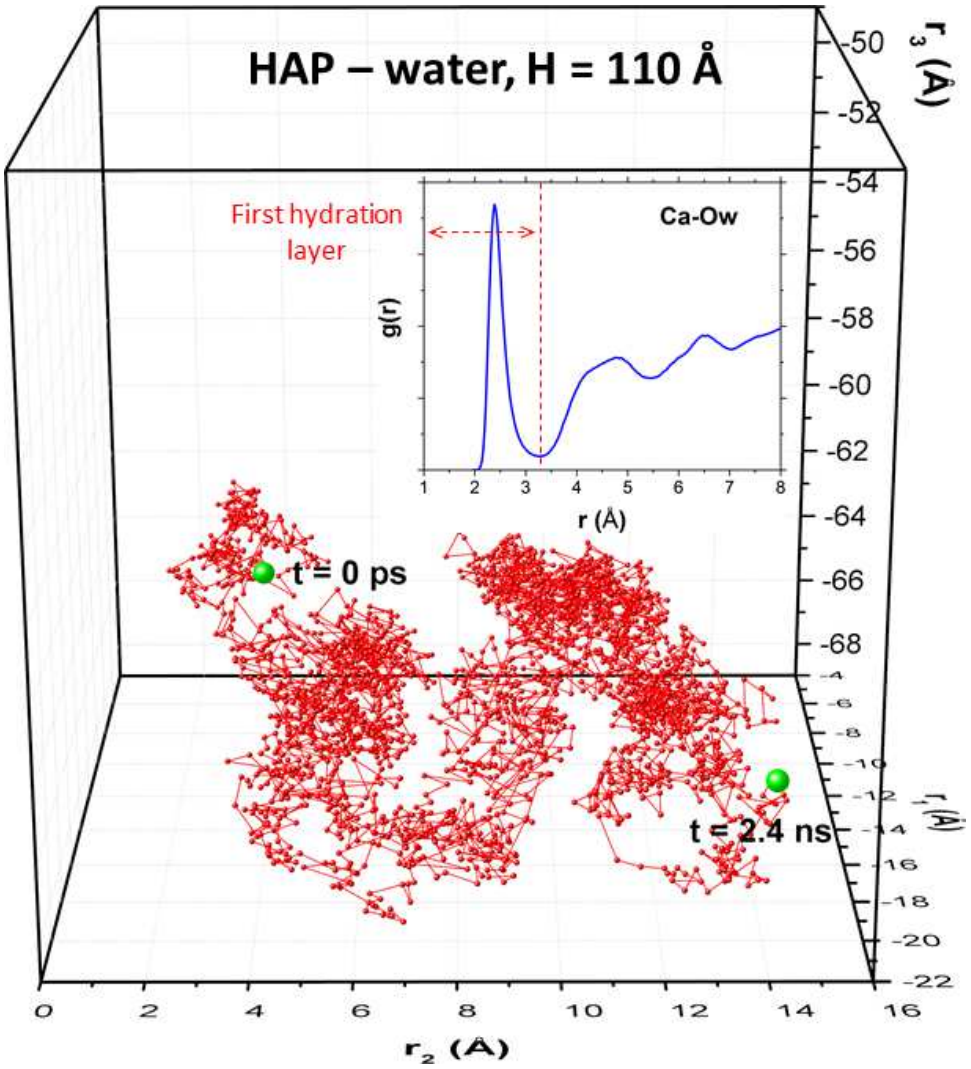

Fig. 5 Motion of a randomly chosen tracer molecule that is part of the first hydration layer of the HAP nanopore with $H = 110$ Å. The inset reports the radial distribution function [g(r)] of calcium ions at the surface and oxygen atoms in water (Ca-Ow).

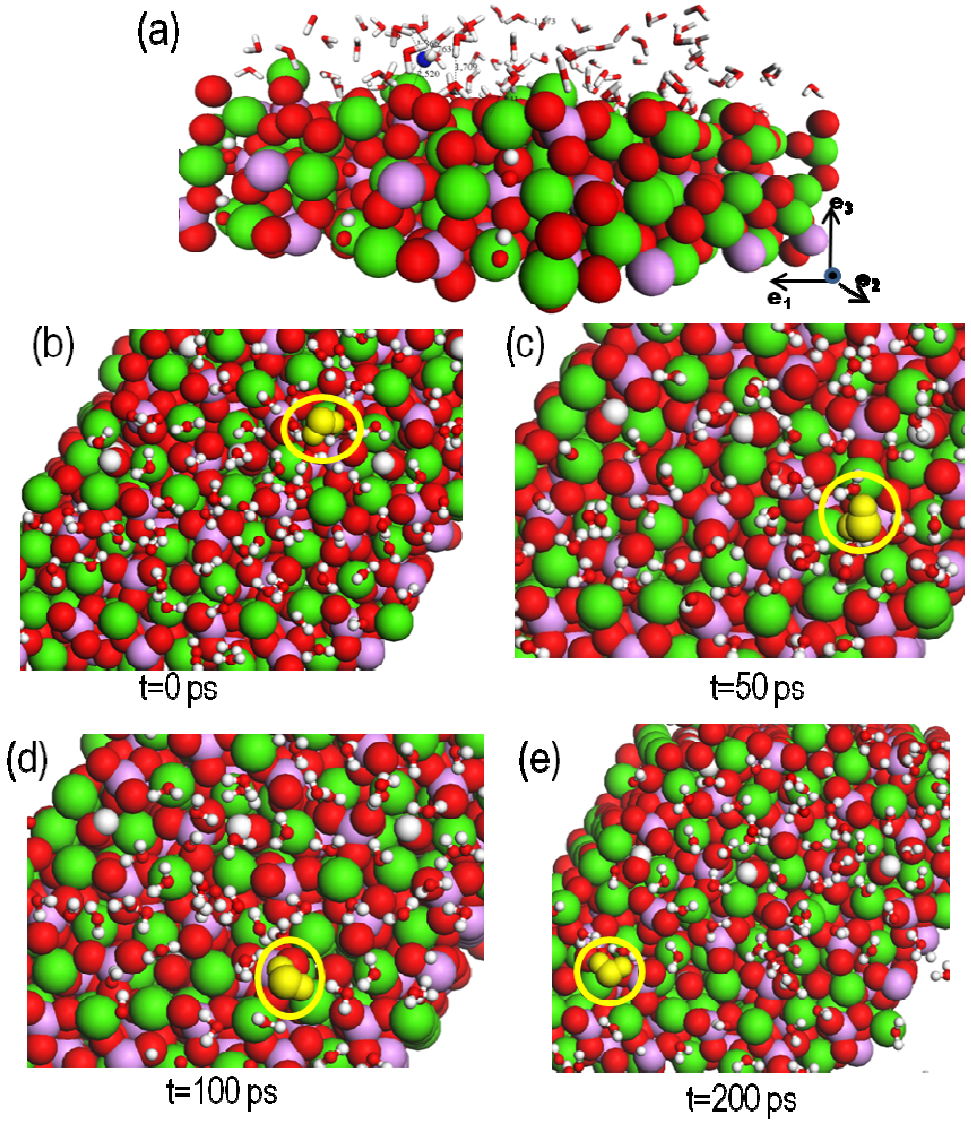

Fig. 6 Molecular arrangement of water molecules on the HAP surface with $H = 70$ Å (Ca-green, P-pink, O-red, H-white and hydroxyl O in blue): (a) H-bonding between hydroxyl ion (HAP) and water molecules: (b) to (e) Motion of selected water molecule (in yellow color circle) on the HAP surface at selected times (in ps).

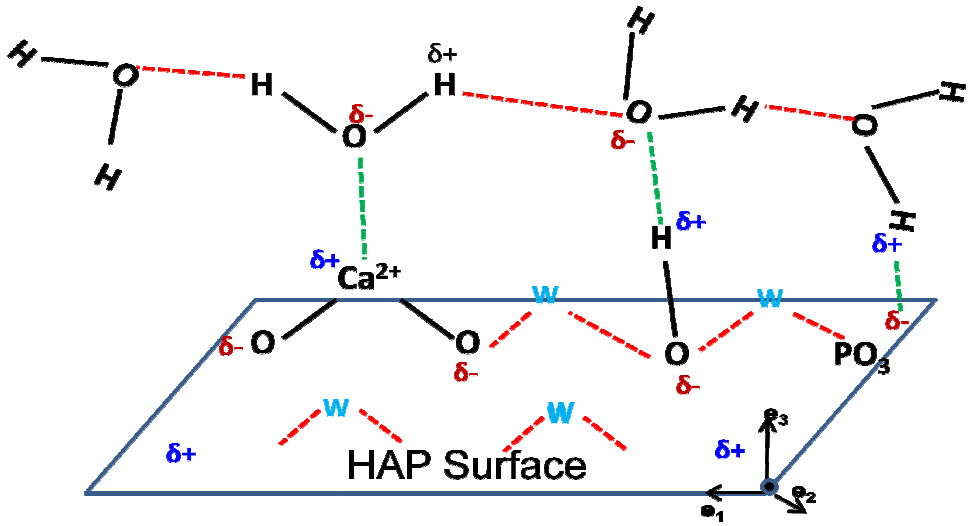

Fig. 7 Schematic representation of the HAP-water interface showing the water adsorption sites and the mechanism of water rolling motion on the HAP surface.